Journal of MATERIALS RESEARCH

Article
DOI:10.1557/s43578-021-00224-3

MULTI-MATERIAL ADDITIVE MANUFACTURING

FOCUS ISSUE

Additive manufacturing of embedded carbon nanocomposite structures with multi-material digital light processing (MMDLP)

SeungYeon Kang[1,2,3], Shing-Yun Chang[2,3], Antonio Costa[4], Kavin Kowsari[2,3], Anson W. K. Ma[2,3,a)]

[1] Department of Mechanical Engineering, University of Connecticut, Storrs, CT 06269, USA
[2] Department of Chemical and Biomolecular Engineering, University of Connecticut, Storrs, CT 06269, USA
[3] Polymer Program, Institute of Materials Science, University of Connecticut, Storrs, CT 06269, USA
[4] Department of Pharmaceutical Sciences, University of Connecticut, Storrs, CT 06269, USA
[a)] Address all correspondence to this author. e-mail: anson.ma@uconn.edu

Received: 6 January 2021; accepted: 27 April 2021

Additive manufacturing (AM) has become an increasingly powerful technique for fabricating complex three-dimensional micro-architectures for a wide variety of applications. Despite the multitude of AM techniques that support single material printing at progressively higher throughput, larger build size, and finer spatial resolution, multi-material printing of interlaced structures with one of the materials being a filled composite has not been demonstrated. This work aims to demonstrate the technical feasibility of fabricating such heterogeneous structures using a custom-built multi-material digital light processing (MMDLP) 3D printer. The printer was equipped with two resin dispensers and an air-jet that enable fast exchange between the resins—one of which was filled with carbon nanotubes (CNTs) up to 0.25%. The inclusion of CNTs reduced the cure depth of the resins, but significantly lowered the critical exposure required to initiate the photopolymerization. This information was successfully used to select appropriate process parameters for printing complex CNT-filled multi-material structures.

Introduction

Additive manufacturing (AM) methods are rapidly gaining interests as alternative methods to conventional nano-, micro-fabrication methods, allowing rapid prototyping of complex freeform geometries from nano- to macro-scales [1, 2]. Accordingly, further development of AM methods is crucial to meet the recent demands for high-throughput, high resolution multi-material printing of high-performance composites, in a low-cost manner [3–5]. Multi-material printed structures with high-performance composites benefit from integration of different functional components and offer a multitude of mechanical, electrical, optical, chemical or biological properties that are not possible for single material systems [5–8]. Despite the variety of techniques, current available AM methods are often costly, have low resolution, are inherently restricted to single material fabrication and require further post-processing to incorporate more than one material [1, 9, 10]. Among the various subsets of AM techniques, photopolymerization-based 3D printing can be a valuable method to resolve the problems [11, 12]. In this technique, photons are used to trigger localized free radical photopolymerization, which converts liquid photopolymer precursors into solid objects by connecting low molecular weight monomers and oligomers to form solid 3D networks [1, 12–14]. Notable recent applications of this technique include multiscale lattice metamaterials [7, 15], tomographic reconstruction [16], 3D printed artificial axons [17], superhydrophobic functional surfaces [18], recyclable thermoset [19], and many others [13–15, 20–26]. The use of light as the primary printing mechanism with a layer-by-layer approach enables relatively high speed and high resolution printing, compared with other AM techniques that are typically based on a point-by-point approach [20, 27].

With the latest technological advancements, digital light processing (DLP) methods show great promise in multi-material

printing of high-performance composites. DLP—a sub-category of photopolymerization-based technique uses ultraviolet (UV) or near-UV to project images on to the photopolymer resin. Figure 1 compares throughput and resolution of various 3D printing techniques with estimated costs. The figure is based on current 3D printing methods that are largely developed for single material or single composite materials. For comparison, the region that corresponds to the MMDLP method presented in this paper is highlighted with a small black dash circle. With further development in the MMDLP technique, the region will likely move towards the left where it is highlighted with a larger black dash circle. Due to the relatively low cost, high-throughput and high resolution printing aspects, DLP can be a viable method for future AM when combined with the potential to print multi-material composite structures.

There have been innovations, such as continuous liquid interface production (CLIP) [20] or volumetric fabrication through holographic patterned images that allow orders of magnitude increase in speed for a faster printing [27]. In the research area of high-performance composite printing of materials, there have been advances in carbon- or glass-filled UV-curable materials in DLP-based 3D printing which include the use of fillers, such as carbon fibers and carbon nanotubes (CNTs) [31–34], nanowires [35], silica [36, 37], iron oxide [38], or graphene oxide (GO) [39], either dispersed in acrylate- or epoxy-based photopolymer matrices for printing single-material objects and precursors that can be further sintered to produce ceramic parts [40]. However, it is important to note that these innovations lack the capability to perform multi-material printing and are limited to printing structures with a single composite material. In this paper, we define multi-material printing as a method to fabricate structures from more than one resin. The printed structures consist of complex interlaced structures, in which the material composition may vary both vertically and laterally, rather than relatively simple stratified multi-material structures.

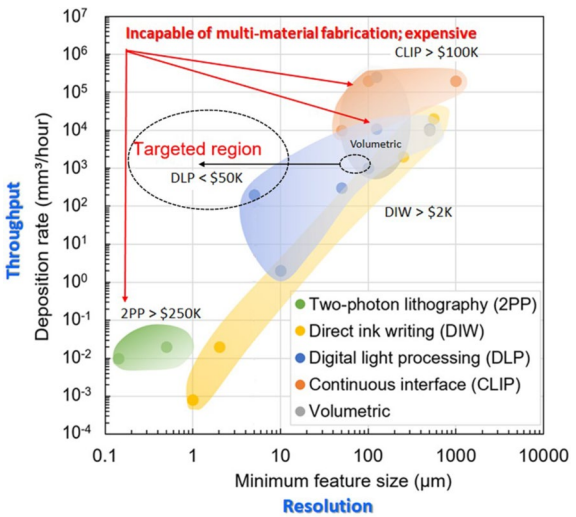

Figure 1: Throughput versus resolution of various additive manufacturing methods with estimated costs, largely based on single or single composite material fabrication. The region that corresponds to the multi-material digital light processing (MMDLP) method presented in this paper is highlighted with a small black-dash circle. With further development in the MMDLP technique, the region will likely move towards the left where it is highlighted with a larger black-dash circle. The figure was adapted from Shusteff.[27] Cost data were collected from independent online databases and journals[28–30].

Our work aims to demonstrate the technical feasibility of producing interlaced composite structures from two resins with one of the resins containing carbon nanotubes (CNTs) as fillers. Previous studies rely on the use of single composite material resins [32–34] and have low resolution on the order of several millimeters to centimeters [32, 34]. By combining an advanced multi-material DLP printing method with studies on carbon-filled photopolymers, we demonstrate the capability of fabricating carbon nanocomposite multi-material structures with a custom-built MMDLP 3D printer. The MMDLP printer is based on a recent study that uses an air-jet to remove the uncured photopolymer resin to prohibit mixing of different resins when more than one resin is used for multi-material printing [41]. Employing this method obviates multiple resin containers or a rotating wheel with different materials and also the use of cleaning solutions or a sonication-assisted brushing process for removing the uncured resin. These processes often result in damages to the printed features and are relatively slow for fabricating complex multi-material parts [34, 41]. Two different types of CNTs were evaluated in terms of their dispersion quality. The cure depths at different CNT concentrations were measured and used to determine the appropriate printing parameters for the additive manufacturing of interlaced carbon nanocomposite structures.

Results and discussion

Figure 2 shows the basic components of the custom-built MMDLP printer. Photocurable resins of the user's choice are loaded into the syringes and then pumped onto the glass plate with software controlled linear stages. The deposited resins are then subjected to UV projections in an upward direction from the DLP light engine through a borosilicate glass plate. A condenser lens is inserted in between the light engine and the glass plate for high resolution printing. The glass plate is covered with an optically clear polytetrafluoroethylene (PTFE) silicone-adhesive tape on the surface to facilitate the separation of the printed layers from the glass plate and for the consecutive new layers to adhere to the printing platform instead of the glass plate. The plate is horizontally translated using a translational stage for re-depositing the resins after each printing step and for positioning the resin puddles to the build platform for the actual printing step. An air-jet is blasted through a tubing placed

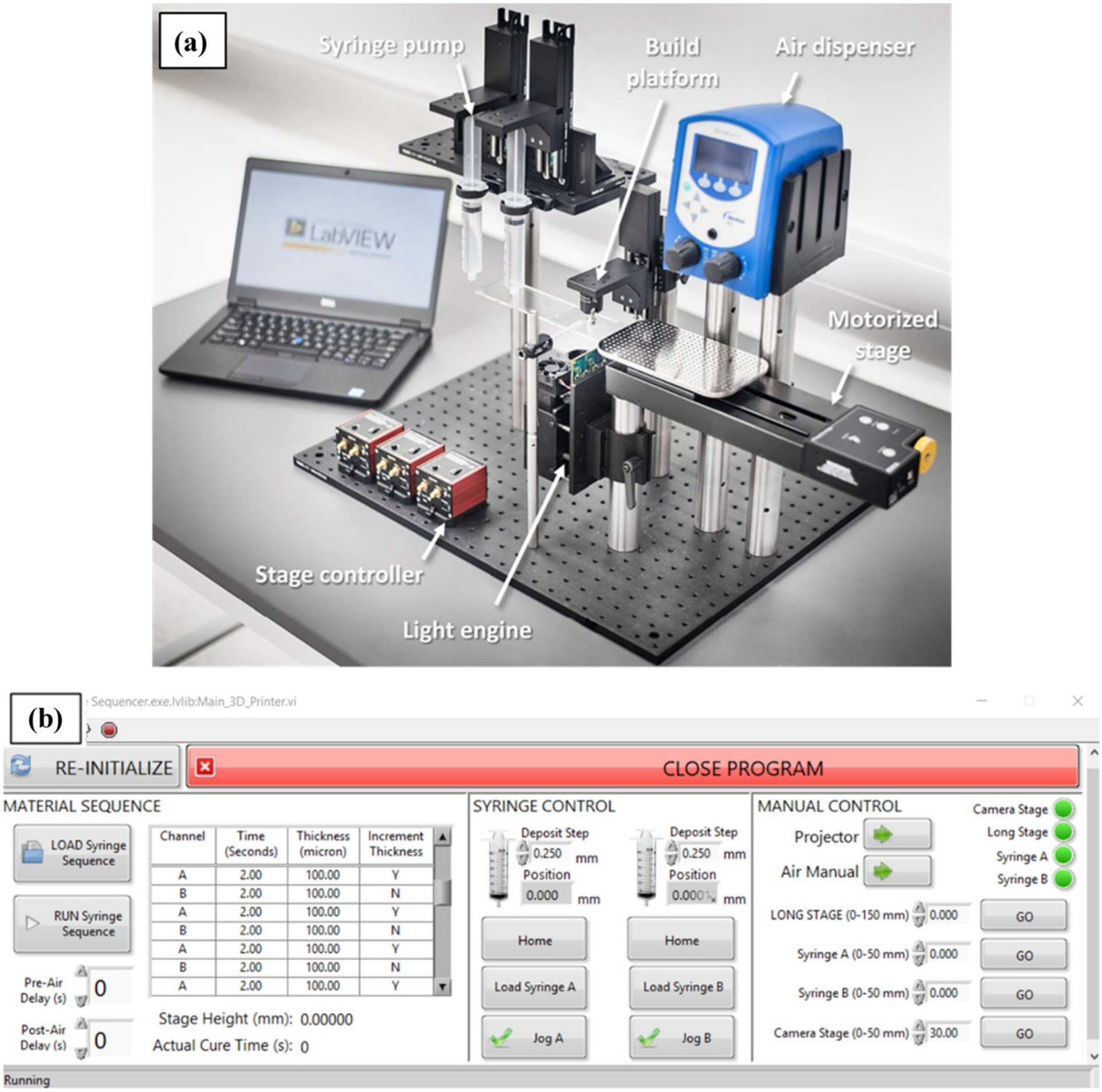

Figure 2: (a) Image of the MMDLP 3D printer used in this study. (b) Graphical user interface of the printer developed using LabVIEW.

a few centimeters away from the build platform to remove the uncured resin.

Laboratory Virtual Instrument Engineering Workbench (LabVIEW) was used to develop the graphical user interface. The interface allows the user to initialize syringes and stages, to load and discharge syringes, to upload and run print parameter files, and to trigger the DLP UV projector. The user interface software has the capability to adjust four parameters; (i) from which of the two syringes the material be dispensed, represented as channel A or B. (ii) an exposure time that can be adjusted between 500 ms and 60 s, (iii) the thickness per print layer ranging from 10 to 1000 μm, and (iv) an "increment thickness" option, where with a Boolean input of Y, the build platform stage will move incrementally according to the set thickness input and with a Boolean input of N, the stage will not increase and remain at the same height allowing the other material to be printed on the same plane.

Figures 3 and 4 illustrate the 3D printing process. Figure 3a and b are images of the MMDLP 3D printer with example inks, red in channel A and blue in channel B. Figure 3a shows dispensing of both ink A and B. A mixture of water and common food dyes were used to illustrate the print process. After the inks are dispensed, the glass plate moves horizontally back to the build platform position. Figure 3b

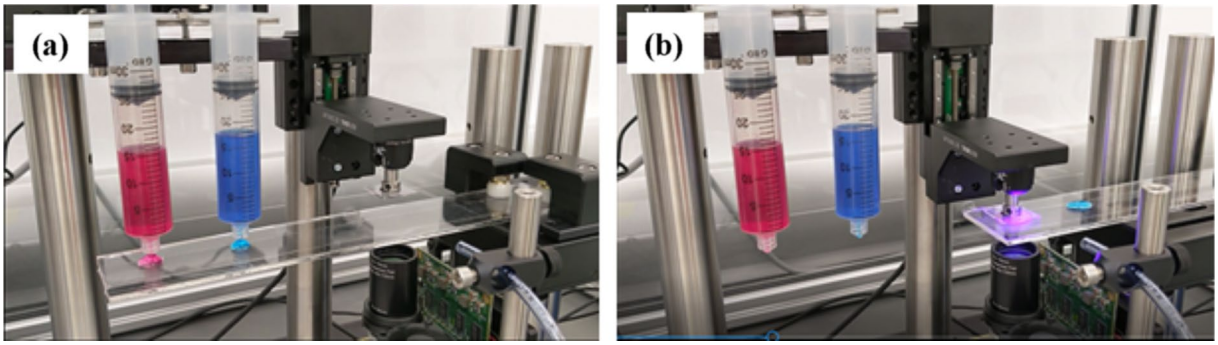

Figure 3: Illustration of the 3D printing process using food dye inks: (a) dispensing of both red (channel A) and blue inks (channel B); (b) lowering of the build plate and projection onto the red ink puddle.

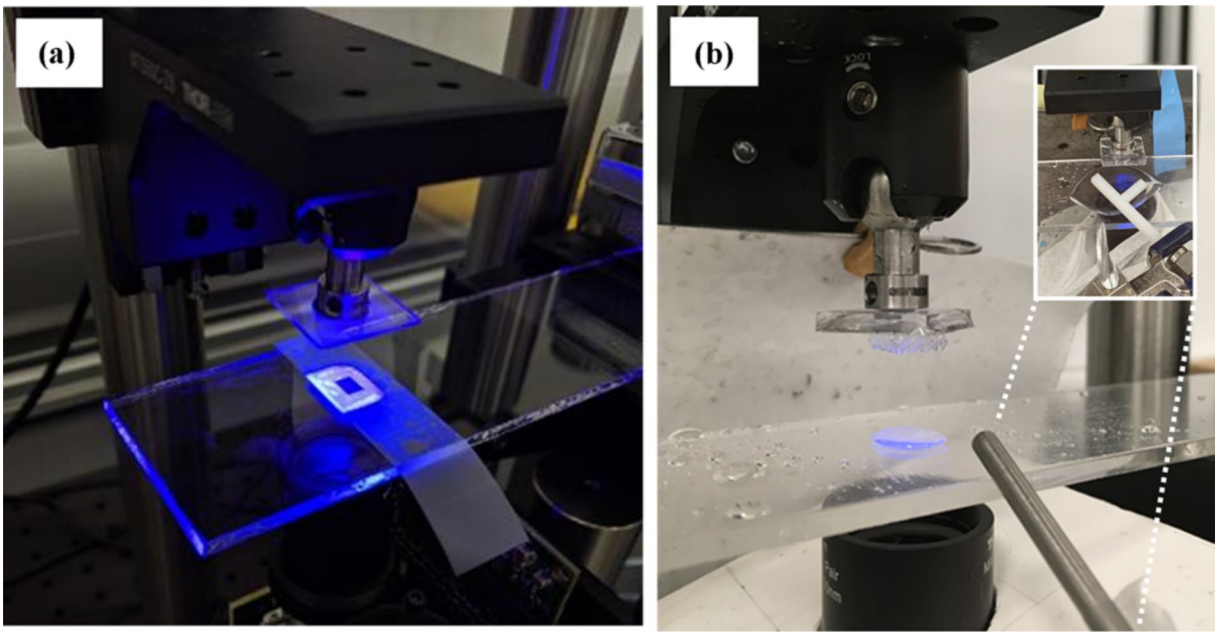

Figure 4: Example of the 3D printing process (a) projection of a square window image with 405 nm UV light from the bottom. A piece of Scotch tape was used to aid the visualization of the projected pattern, (b) a representative example of a 3D printed structure after removing excess photopolymer resin with an air-blower. Basic Formlabs Clear resin, without CNTs, was used. The inset image shows an interchangeable right-angled air distributor.

shows an instance where the build platform is lowered to a desired height for initiating photopolymerization process using ink A. After a layer is printed with ink A, the air-jet removes the uncured ink A and the glass plate moves to the ink B puddle position to proceed with the following printing step with ink B. At this stage for printing multi-material structures on the same layer, the build plate form is lowered to the previous identical height. Once the printing with ink B is done, the glass plate moves horizontally back to the ink dispensing position to re-deposit the inks. Figure 4a and b are images of the actual printing process. Figure 4a shows an instance of a square window image that was projected for patterning with a 405-nm UV light from the bottom projector. Scotch tape was used to allow visualization of the projected pattern without any ink sample. Figure 4b shows an example of a 3D printed structure adhered to the build platform after removing the excess ink material with an air-blower. The remaining ink puddle on the bottom glass plate can be reused for printing the following layers minimizing the ink wasted during the process. The inset image on the right shows an instance when an interchangeable right-angled air-blower tip has been inserted that has been designed to increase the efficiency of the excess ink removal process. Effective removal of the excessive ink remains an on-going study as it requires careful optimization of the air flow rate to ensure that the drag forces induced by the air flow is sufficient in overcoming viscous and surface forces of the resin without deforming the printed structure. As a final step, the fully printed structures

are rinsed in ethanol for 10 s to further remove any uncured ink material that may remain trapped within the structures after the air-jet treatment.

CNT was chosen as an example filler material due to the additional electrical, thermal, mechanical, and optical functionalities it can potentially impart to the printed structures [32–34, 42]. Two common types of CNTs, namely, CoMoCAT® and CVD, were studied. These CNTs have similar lengths, but CVD CNTs have an average diameter that is an order of magnitude larger than CoMoCAT®. Of particular interest is how the CNT diameter may influence the quality of CNT dispersion in the photopolymer resins. To assess dispersion quality, CNT were dispersed in poly (ethylene glycol) methyl ether methacrylate (PEGMEMA), a base material for custom-made resins [32] (Supplementary Fig. 1) and a commercial Formlabs Clear resin, respectively. Figure 5a compares the optical micrographs of the two types of CNTs dispersed in Formlabs clear resin after 30 min of sonication. The CNTs synthesized from the CoMoCAT® technique formed a gel-like suspension (left), while the CNTs synthesized with the CVD technique formed a more uniform dispersion (right). As shown in the microscopic images, the gel-like suspension from the CoMoCAT® CNTs contains many large agglomerates (Fig. 5b), while the dispersion of CVD CNTs shows well dispersed clusters of needle-like CNTs (Fig. 5c). The poor dispersity of CoMoCAT® CNTs is likely caused by the high aspect ratio and small diameter which induces significant entanglement of CNT, leading to agglomerates [43]. Choosing a filler material with minimal or no agglomeration is important not only to achieve homogenous properties within a printed structure but also to minimize interference with the propagating UV light and to allow printing of thinner layers which leads to reduced overall surface roughness of the final structure. In cases where a print layer thickness of 100 μm or less is used for printing, the regions with large CoMoCAT® CNT agglomerates in Fig. 5b will likely suffer from poor adhesion to the previously printed layer due to the lack of photocurable base resin. The interlayer defects caused by improper adhesion between the layers and uneven layers from protruding agglomerates would result in overall mechanical weakness of the printed structure. The undesirable rough staircase like surface features caused by printing with larger print layer thicknesses is discussed further in the final results section of this paper. Therefore, in this study, we chose the CNTs made from the CVD method to be used as the filler material to be dispersed in the base photopolymer resin.

Identification of optimum filler loading is important not only to guarantee homogeneous dispersion, but also to determine the necessary UV exposure time required for a desired curing thickness. Therefore, we carry out curing depth measurements to find out the minimum exposure time needed to cure a given thickness of photopolymer, and to determine the minimum energy the photopolymer needs to initiate the

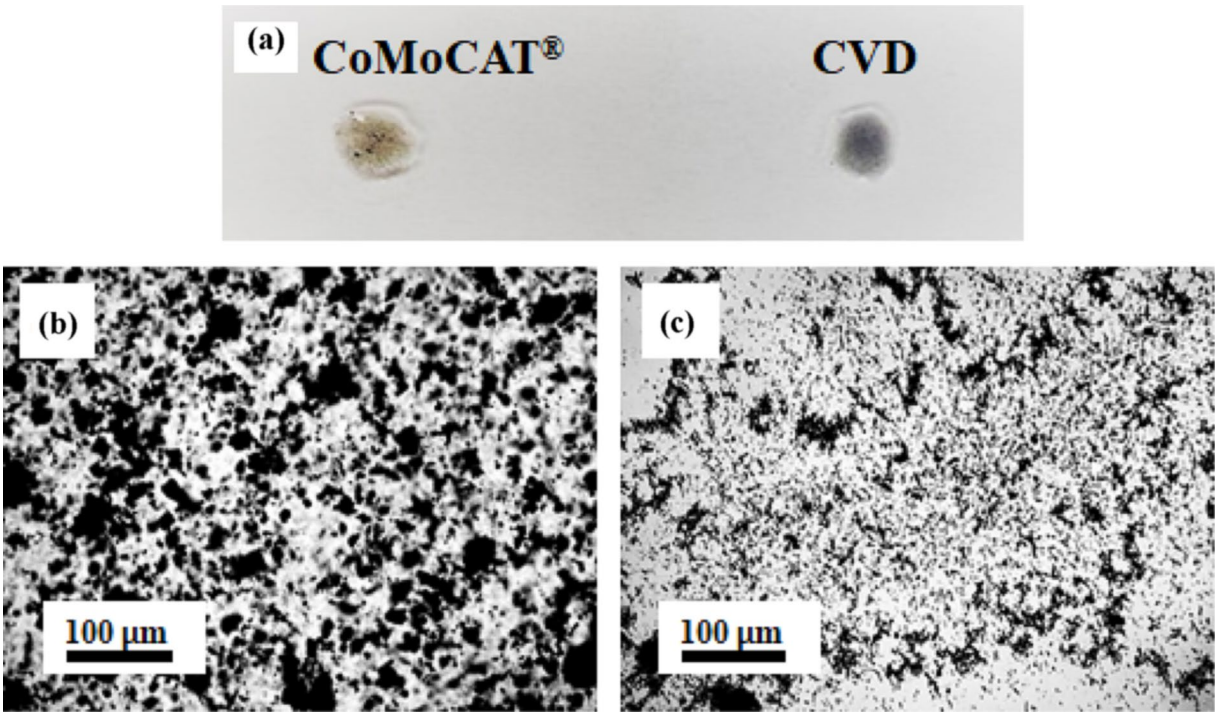

Figure 5: Macroscopic (a) and microscopic images (b, c) of Formlabs clear resin containing 0.5% (w/w) CNTs synthesized by (b) CoMoCAT® and (c) CVD technique, respectively.

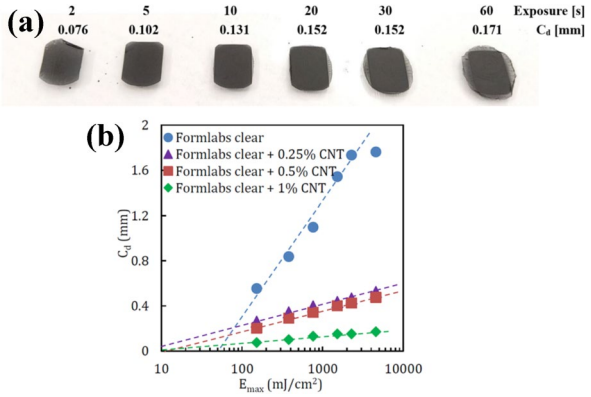

Figure 6: (a) Formlabs clear resins containing 1% (w/w) CNT, exposed to the UV light of the 3D printer for 2, 5, 10, 20, 30 and 60 s, respectively from left to right (b) Working curves (dashed lines) of Formlabs clear photopolymer resins containing different CNT concentrations.

polymerization reaction. The thickness measured from the cured resins with different exposure times represents the curing depth with respect to various energies applied. The clear PTFE tape showed negligible absorption and a UV intensity of 76 mW/cm^2 was measured at the interface where the photopolymer is deposited. We assume that as soon as a UV pattern is projected, the polymerization happens from the bottom of photopolymer resin puddle and proceeds upwards.

Figure 6b presents cure depth versus UV exposure intensity working curve graphs plotted from measuring the thickness of cured CNT-dispersed (1% w/w) Formlabs clear resins with UV exposure times of 2, 5, 10, 20, 30 and 60 s, as shown in Fig. 6a. As the exposure time increases, not only the thickness of the cured polymer increases but also polymerization occurs laterally resulting in a decrease in print resolution. Therefore, it is important to determine the optimum exposure time that does not under-expose or over-expose the resin. Further, no noticeable difference in cure depth was noted at different locations within the same sample, confirming the uniformity of the UV intensity within the projected area. The larger cured area compared to the projected area was likely caused by internal scattering and change in refractive index as polymerization progressed. Similar observations also have been reported in Ref. [44].

The working curve of the CNT-dispersed photopolymer resin was generated and fitted using the working curve equation (Eq. 1).

$$C_d = D_p ln\left(\frac{E_{max}}{E_c}\right) \quad (1)$$

where C_d is the curing depth, D_p is the penetration depth of the resin, and D_p is defined as $D_p = 1/(2.3\varepsilon[I])$. Here, ε is the molar extinction coefficient of the initiator (L/mol*cm) and [I] is the initiator concentration (mol/L). E_{max} is the UV exposure intensity (mJ/cm^2) at the resin interface which can be calculated by exposure time, in seconds, multiplied by 76 mW/cm^2, which was measured using a UV power meter. E_c is the critical exposure intensity (mJ/cm^2) of the resin at the UV wavelength, which in other words is the minimum light energy required to initiate polymerization. Derived from the Beer-Lambert law, this equation shows that the curing depth is proportional to the natural logarithm of the maximum exposure intensity of UV light. Subsequently, a semi-log plot of cure depth versus exposure generates working curves shown as dashed lines in Fig. 6b for a given photopolymer. The working curves are generated only from the data in the linear regime where light scattering effects are minimal as a result of refractive index changes during the polymerization process. Previous studies have shown that the equation fails at high energy exposures resulting in saturation of the curing depth [45]. The penetration depth (D_p) can be obtained from the slope of the curves and the critical exposure (E_c) can be obtained from the x-intercepts on the graph.

The values acquired from the working curves are tabulated in Table 1. Penetration depth, D_p, and critical exposure, E_c, are inherent properties of each material. As one can see from comparing the values in Table 1, the inclusion of CNTs reduces the values of D_p due to the strong UV absorption characteristic of CNTs, which is a common phenomenon also occurring in other nanofillers as well [46]. However, CNTs also significantly decrease the E_c of resin for triggering of photopolymerization. Similar findings have been reported in previous studies where CNT-filled UV curable composites were investigated [47]. Upon photo-excitation, the semiconducting behavior of CNTs generates an electron and a hole in conduction and valence bands, respectively. Both holes and electrons induce radicals from acrylic monomers through oxidation and reduction. As a result, in addition to the added photoinitiator, more radicals are present to initiate photopolymerization at lower energy levels [47]. Using Eq. 1 and the parameters in Table 1, minimum exposure times required for different layer thickness were calculated and shown in Table 2. These values are used as guiding principles in the actual 3D printing process.

Figure 7 and Supplementary Fig. 3 show successful fabrication of complex multi-material 3D DLP printing, in which

TABLE 1: Penetration depth (D_p) and critical exposure intensity (E_c) obtained from fitting cure depth data to working curve Eq. (1).

	D_p (mm)	E_c (mJ/cm^2)
Formlabs clear resin	1.02	51
Formlabs clear + 0.25% CNT	0.17	4
Formlabs clear + 0.5% CNT	0.18	11
Formlabs clear + 1% CNT	0.07	8

TABLE 2: Minimum exposure time required to obtain cured resin with a thickness of 25, 50 and 100 µm, respectively.

	Minimum exposure time (s)		
	25 µm	50 µm	100 µm
Formlabs clear resin	0.70	0.75	0.83
Formlabs clear + 0.25% CNT	0.07	0.10	0.20
Formlabs clear + 0.5% CNT	0.18	0.24	0.46
Formlabs clear + 1% CNT	0.32	0.72	3.73

the material composition varies in both vertical and lateral directions. Structures in Fig. 7 were printed with the carbon nanocomposite resin in which the black parts are composed of layers printed using 0.25% (w/w) carbon nanotubes dispersed in Formlabs clear resin. The clear parts are composed of layers printed with the original Formlabs clear resin for visual contrast. A thick sacrificial layer was printed initially as a foundation for the structures. The CNT composite structures presented in this paper have features on the order of hundreds of micrometer—higher resolution than those previously reported in the range of several millimeters to centimeters [32, 34]. All structures have been printed with a build platform step height of 100 µm for faster printing. Figure 7a shows a 4-layer multi-material polyhedron ProFab© lattice structure where each unit cell is composed of fourteen rhombic and hexagonal faces. Each interchanging colored-layer comprises 28 consecutive print layers. Figure 7b shows a simple cubic lattice structure with a carbon nanocomposite rod embedded in the middle and Fig. 7c shows high aspect ratio hair-like structures, also with a carbon nanocomposite rod in the middle. Structures presented in Figs. 7b and c demonstrate the capability to print two different materials laterally, allowing the 3D printing of complex embedded features. A close-up image of a single rod is inserted on the right of Fig. 7c which shows a rough surface with a staircase like feature. The DLP printing process is inherently a resin solidification process in the vertical direction and therefore results in sloped vertical-edge structures from decreasing light intensity along the propagation path [41]. In our custom-built MMDLP printer, the solidification (i.e., polymerization) begins to occur at the glass–liquid interface at the bottom, then propagates upward toward the printing platform at which the solidified layer adheres to the previously printed layer. The reduced light intensity and therefore the reduced solidification process towards the top leads to trapezoidal-shaped printed layers with narrower side at the top which collectively result in a rugged step surface. Note that the build platform is at the top in our setup producing structures in an upside-down manner. Structures in Fig. 7 have been flipped over to their correct upright position and therefore has the wider side of a trapezoid at the top as in the inset Fig. 7(c). With high resolution vertical step motors one can choose to use a build platform step height of far less than 100 µm, however, at the sacrifice of the total print time.

Conclusions

In this paper, a low-cost, multi-material digital light processing (MMDLP) 3D printer has been designed and custom-built for fabricating complex carbon nanocomposite structures with a minimum feature size on the order of hundreds of micrometers. The MMDLP printer employs a dual-syringe configuration with an air-jet nozzle to facilitate transition between two photopolymer resins. One of the resins was filled with carbon nanotubes (CNTs). CNTs synthesized by two different methods, namely CoMoCAT® and CVD, were investigated. CVD CNTs tend to have better dispersion characteristics compared to CoMoCAT® that are smaller in diameter and tend to bundle via van der Waals interactions. The CVD CNTs were further dispersed at different concentrations in a commercial resin from Formlabs. Penetration depth decreased as a function of increasing CNT concentration in the base photopolymer resin. Interestingly, the critical exposure intensity was found to decrease as the CNT concentration increased, which may be explained

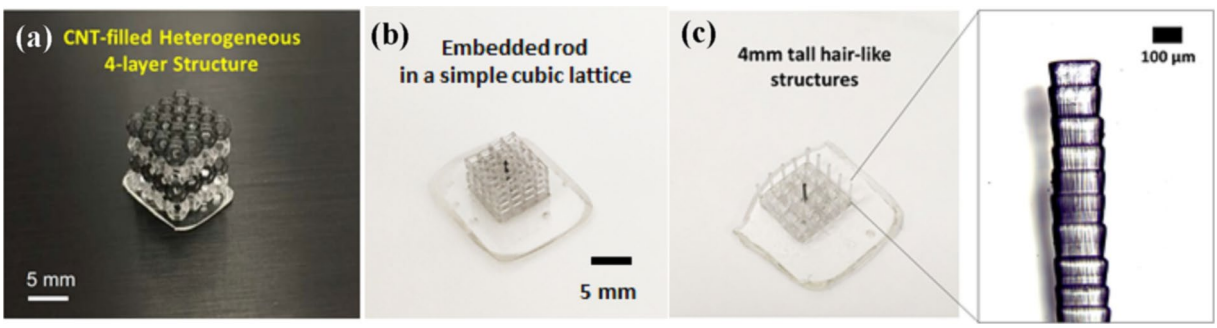

Figure 7: Complex MMDLP printing with carbon nanocomposites with black layer composed of 0.25% (w/w) carbon nanotubes dispersed in Formlabs clear resin. All structures include a thick sacrificial layer printed initially at the base. (a) a 4-layer multi-material polyhedron ProFab © lattice structure, (b) simple cubic lattice structure with a carbon nanocomposite rod embedded in the middle, (c) 180 µm × 180 µm base, 4 mm height square rods with a carbon nanocomposite rod in the middle. Picture inserted on the right shows a close-up image of a single rod.

by the generation of free radicals due to CNTs' semiconducting properties. The successfully printed structures consist of interlaced composite structures, in which the material composition may vary both vertically and laterally, rather than relatively simple stratified multi-material structures. Our work successfully demonstrates the technical feasibility of producing complex multi-material composite structures from two resins with one of the resins containing carbon nanotubes (CNTs) as fillers. The presented MMDLP printing method opens up the exciting possibility of creating intricate composite structures from multiple resins that are individually formulated but are seamlessly integrated through the print process. Such capability is important for increasing the degree of freedom in print design because the overall properties can be engineered by changing the topology as well as the local material composition on the voxel-level, further enabling novel 3D printed parts that are topologically and functionally optimized with unprecedented properties.

Experimental procedure

Materials

Multiwall CNTs synthesized by two different methods, namely CoMoCAT® and chemical vapor deposition (CVD), were investigated. CoMoCAT® CNTs (Sigma-Aldrich 773,840) have an outer diameter of 10 nm and a length of 3 – 6 μm. CVD-synthesized CNTs (Sigma-Aldrich 659,258) have a diameter of 110 – 170 nm and a length of 5 – 9 μm. The CNTs were used without further purification or chemical treatment. For CNT dispersion studies, poly (ethylene glycol) methyl ether methacrylate (PEGMEMA, average Mn = 500 g/mol), a less hazardous solvent that was reported for having a good dispersion of CNTs [32] and a commercial Formlabs Clear resin (FLGPCL04) have been used. For working curve studies and subsequent 3D printing of the complex structures, Formlabs Clear photopolymer resin has been chosen as the base photopolymer resin. This resin is transparent, allowing for easy visualization of the multi-material structures printed from the clear neat resin and the dark resin filled with CNTs. For illustration of the printing process in Fig. 3, red and blue food dyes were purchased from McCormick & Co., Inc.

CNT dispersion preparation

Different amount of CNT, ranging from 0.25% to 1% (w/w), was dispersed in 30 mL of poly (ethylene glycol) methyl ether methacrylate (PEGMEMA) or Formlabs clear resin using sonication (BRANSON 450) at 30% of maximum intensity for at least 30 min. The highest CNT concentration (1%) requires a longer sonication time up to 1 h. Sonication was followed by high shear mixing (homogenizer IKA T18) at 3000 rpm for 5 min. Ambient light exposure was minimized during the preparation of CNT dispersions.

MMDLP printer components

UV light for photopolymerization is projected upward from the DLP light engine (CEL5500, Digital Light Innovations, Austin, TX) through a 400 × 50 x 5 mm borosilicate glass plate. A condenser lens is inserted in between the light engine and the glass plate covered with an optically clear polytetrafluoroethylene (PTFE) silicone-adhesive tape. The plate is horizontally translated using a translational stage (LTS150, Thorlabs, Inc., Newton, NJ) for positioning the resin puddles to the build platform for printing and for replenishing the resins if needed. For removing uncured resins, 5 s of a 250 kPa air-jet is blasted through a 2 mm diameter steel tubing placed a few centimeters away from the build platform. The steel tubing can be switched to a specifically designed air distributor (Fig. 4b) to improve the air-jet coverage. The interchangeable air distributor was 3D printed using Connex3 Objet350 printer with Digital ABS resin (Stratasys Ltd.) and has a right-angled blowing tip with two 1 mm × 1 mm square openings at each end.

Cure depth measurements

To measure the curing depth, the neat and CNT-filled photopolymer resins were exposed to UV for different times ranging from 2 to 120 s. After washing away the uncured photopolymer with ethanol, the thickness of the remaining cured samples was measured using a caliper. The intensity of the UV light source at the printing position was measured with a portable UV power meter (Model 308 UV Light Meter, Optical Associates, Incorporated., CA)).

Acknowledgments

This material is based upon work supported by the National Science Foundation under Grant No. IIP-#1822157 (Phase I IUCRC at University of Connecticut: Center for Science of Heterogeneous Additive Printing of 3D Materials (SHAP3D)) and from the SHAP3D I/UCRC Members: Akita Innovations, Boeing Company, U.S. Army CCDC Armaments Center, U.S. Army CCDC Soldier Center, Desktop Metal, HP Inc, Hutchinson, Integrity Industrial Ink Jet Integration LLC, Karagozian & Case, Raytheon Technologies, Stratasys Ltd, and Triton Systems Inc. Any opinions, findings, and conclusions or recommendations expressed in this material are those of the author(s) and do not necessarily reflect the views of the National Science Foundation or the sponsors. The authors would like to thank the industry advisory board members, Dr. Patrick Kinlen, John

Sailhamer, Dr. Scott Eastman, and Dr. Adam Pawloski for their technical inputs and Joseph Luciani for assistance with printing the air distributor.

Author contributions

SK and S-YC performed the experiments and data analysis. KK contributed to the initial construction of the MMDLP 3D printer. The graphical user interface was developed by AC. KK and AWKM were responsible for the conceptualization, funding acquisition, and project administration. SK was the primary author of the manuscript, which was reviewed and edited by all the co-authors.

Declarations

Conflict of interest The authors report no declarations of interest.

Supplementary Information

The online version contains supplementary material available at https://doi.org/10.1557/s43578-021-00224-3.

References

1. H. Lipson, M. Kurman, *Fabricated: The New World of 3D Printing* (Wiley, New York, 2013).
2. H. Bikas, P. Stavropoulos, G. Chryssolouris, Additive manaufacturing methods and modeling approaches: a critical review. Int. J. Adv. Manuf. Technol. **83**, 389–405 (2016)
3. S.C. Ligon, R. Liska, J. Stampfl, M. Gurr, R. Mülhaupt, Polymers for 3D printing and customized additive manufacturing. Chem. Rev. **117**, 10212–10290 (2017)
4. M.A. Skylar-Scott, J. Mueller, C.W. Visser, J.A. Lewis, Voxelated soft matter via multimaterial multinozzle 3D printing. Nature **575**, 330–335 (2019)
5. F. Li, N.P. Macdonald, R.M. Guijt, M.C. Breadmore, Increasing the functionalities of 3D printed microchemical devices by single material, multimaterial, and print-pause-print 3D printing. Lab Chip **19**, 35–49 (2019)
6. A. Kashirina, Y. Yao, Y. Liu, J. Leng, Biopolymers as bone substitutes: a review. Biomater. Sci. **7**, 3961–3983 (2019)
7. D. Chen, X. Zheng, Multi-material additive manufacturing of metamaterials with giant tailorable negative Poisson's ratios. Sci. Rep. **8**, 1–8 (2018)
8. R. Hensleigh et al., Charge-programmed three-dimensional printing for multi-material electronic devices. Nat. Electron. **3**, 216–224 (2020)
9. M. Vaezi, S. Chianrabutra, B. Mellor, S. Yang, Multiple material additive manufacturing: Part 1: a review: this review paper covers a decade of research on multiple material additive manufacturing technologies which can produce complex geometry parts with different materials. Virtual Phys. Prototyp. **8**, 19–50 (2013)
10. M. Nadgorny, A. Ameli, Functional polymers and nanocomposites for 3D printing of smart structures and devices. ACS Appl. Mater. Interfaces **10**, 17489–17507 (2018)
11. M. Layani, X. Wang, S. Magdassi, Novel materials for 3D printing by photopolymerization. Adv. Mater. **30**, 1–7 (2018)
12. X. Zheng et al., Design and optimization of a light-emitting diode projection micro-stereolithography three-dimensional manufacturing system. Rev. Sci. Instrum. **83**, 125001 (2012)
13. Q. Ge et al., Multimaterial 4D printing with tailorable shape memory polymers. Sci. Rep. **6**, 31110 (2016)
14. C. Sun, N. Fang, D.M. Wu, X. Zhang, Projection micro-stereolithography using digital micro-mirror dynamic mask. Sens. Actuators A Phys. **121**, 113–120 (2005)
15. X. Zheng et al., Multiscale metallic metamaterials. Nat. Mater. **15**, 1100–1106 (2016)
16. B.E. Kelly et al., Volumetric additive manufacturing via tomographic reconstruction. Science **363**, 1075–1079 (2019)
17. D. Espinosa-Hoyos et al., Engineered 3D-printed artificial axons. Sci. Rep. **8**, 478 (2018)
18. Y. Yang et al., 3D-printed biomimetic super-hydrophobic structure for microdroplet manipulation and oil/water separation. Adv. Mater. **30**, 1704912 (2018)
19. B. Zhang, K. Kowsari, A. Serjouei, M.L. Dunn, Q. Ge, Reprocessable thermosets for sustainable three-dimensional printing. Nat. Commun. **9**, 1831 (2018)
20. J.R. Tumbleston et al., Continuous liquid interface production of 3D objects. Science **347**, 1349–1352 (2015)
21. F. Kotz et al., Three-dimensional printing of transparent fused silica glass. Nature **544**, 337–339 (2017)
22. Z. Chi, C. Yong, Y. Zhigang, K. Behrokh, Digital material fabrication using mask-image-projection-based stereolithography. Rapid Prototyp. J. **19**, 153–165 (2013)
23. J.-W. Choi, H.-C. Kim, R. Wicker, Multi-material stereolithography. J. Mater. Process. Technol. **211**, 318–328 (2011)
24. C. Zhou, H. Ye, F. Zhang, A novel low-cost stereolithography process based on vector scanning and mask projection for high-accuracy, high-speed, high-throughput, and large-area fabrication. J. Comput. Inf. Sci. Eng. **15**, 10 (2015)
25. M.M. Emami, F. Barazandeh, F. Yaghmaie, Scanning-projection based stereolithography: method and structure. Sens. Actuators A Phys. **218**, 116–124 (2014)
26. X. Zheng et al., Ultralight, ultrastiff mechanical metamaterials. Science **344**, 1373–1377 (2014)
27. M. Shusteff et al., One-step volumetric additive manufacturing of complex polymer structures. Sci. Adv. **3**, 5496 (2017)
28. Senvol database on industrial additive manufacturing machines and materials. http://senvol.com/database/.

29. M. Evan, L. Hod, Fab@Home: the personal desktop fabricator kit. Rapid Prototyp. J. **13**, 245–255 (2007)
30. Aniwaa online platform. https://www.aniwaa.com/comparison/3d-printers/.
31. Z. Xu et al., Additive manufacturing of two-phase lightweight, stiff and high damping carbon fiber reinforced polymer microlattices. Addit. Manuf. **32**, 101106 (2020)
32. G. Gonzalez et al., Development of 3D printable formulations containing CNT with enhanced electrical properties. Polymer (Guildf). **109**, 246–253 (2017)
33. J.H. Sandoval, K.F. Soto, L.E. Murr, R.B. Wicker, Nanotailoring photocrosslinkable epoxy resins with multi-walled carbon nanotubes for stereolithography layered manufacturing. J. Mater. Sci. **42**, 156–165 (2007)
34. Q. Mu et al., Digital light processing 3D printing of conductive complex structures. Addit. Manuf. **18**, 74–83 (2017)
35. Y. Han, F. Wang, H. Wang, X. Jiao, D. Chen, High-strength boehmite-acrylate composites for 3D printing: reinforced filler-matrix interactions. Compos. Sci. Technol. **154**, 104–109 (2018)
36. E. Shukrun, I. Cooperstein, S. Magdassi, 3D-printed organic-ceramic complex hybrid structures with high silica content. Adv. Sci. **5**, 1800061 (2018)
37. Z. Weng, Y. Zhou, W. Lin, T. Senthil, L. Wu, Structure-property relationship of nano enhanced stereolithography resin for desktop SLA 3D printer. Compos. Part A Appl. Sci. Manuf. **88**, 234–242 (2016)
38. Z. Ji, C. Yan, B. Yu, X. Wang, F. Zhou, Multimaterials 3D printing for free assembly manufacturing of magnetic driving soft actuator. Adv. Mater. Interfaces **4**, 1700629 (2017)
39. A. Chiappone et al., Study of graphene oxide-based 3D printable composites: effect of the in situ reduction. Compos. Part B Eng. **124**, 9–15 (2017)
40. C. Wang et al., A general method to synthesize and sinter bulk ceramics in seconds. Science **368**, 521–526 (2020)
41. K. Kowsari, S. Akbari, D. Wang, N.X. Fang, Q. Ge, High-efficiency high-resolution multimaterial fabrication for digital light processing-based three-dimensional printing. 3D Print. Addit. Manuf. **5**, 185–193 (2018)
42. F.H. Gojny et al., Evaluation and identification of electrical and thermal conduction mechanisms in carbon nanotube/epoxy composites. Polymer (Guildf). **47**, 2036–2045 (2006)
43. J. Qian et al., Effect of aspect ratio of multi-wall carbon nanotubes on the dispersion in ethylene-α-octene block copolymer and the properties of the nanocomposites. J. Polym. Res. **26**, 1–11 (2019)
44. K. Kowsari et al., Photopolymer formulation to minimize feature size, surface roughness, and stair-stepping in digital light processing-based three-dimensional printing. Addit. Manuf. **24**, 627–638 (2018)
45. P. Gandhi, K. Bhole, 3D microfabrication using bulk lithography. ASME 2011 Int. Mech. Eng. Congr. Expo. IMECE **11**, 393–399 (2011)
46. P.F. Jacobs, Lasers for Rapid Prototyping & Manufacturing, in *Rapid Prototyping & Manufacturing: Fundamentals of Stereolithography*. (Society of Manufacturing Engineers, Southfield, 1992)
47. M. Sangermano, F. Marino, N. Reuel, M.S. Strano, Semiconducting single-walled carbon nanotubes as radical photoinitiators. Macromol. Chem. Phys. **212**, 1469–1473 (2011)